ADVANCED FUNCTIONAL MATERIALS

Supporting Information

for *Adv. Funct. Mater.*, DOI: 10.1002/adfm.202004615

Photocatalytic Nanowires-Based Air Filter: Towards Reusable Protective Masks

*Endre Horváth, Lídia Rossi, Cyprien Mercier, Caroline Lehmann, Andrzej Sienkiewicz, and László Forró**

Supporting Information

Photocatalytic nanowires-based air filter: towards reusable protective masks

E. Horváth[1], L. Rossi[1], C. Mercier[1], C. Lehmann[2], A. Sienkiewicz[1, 3], L. Forró[1]

[1]Laboratory of Physics of Complex Matter, Ecole Polytechnique Fédérale de Lausanne, 1015 Lausanne, Switzerland

[2]Laboratory of Physics of Living Matter, Ecole Polytechnique Fédérale de Lausanne, 1015 Lausanne, Switzerland

[3]ADSresonances, 1028 Préveranges, Switzerland

1. Structural characterization of the TiO_2NWs-based filter paper

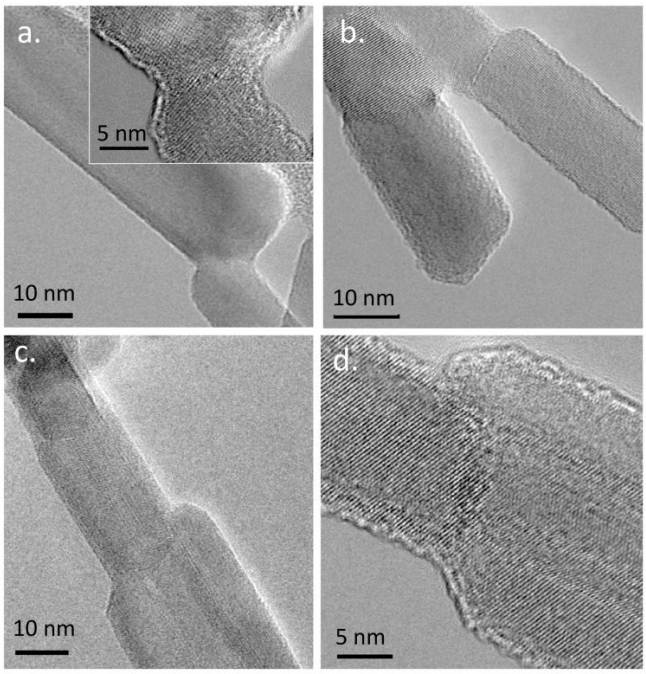

Figure S1. HRTEM micrographs of the fused TiO_2NWs after the calcination process.

Fig. S1 shows high-resolution TEM images of the interconnected TiO_2NWs obtained from the doctor bladed film calcined at 600 ^oC for 2 h. The TiO_2NWs elongated in the [001] direction exhibit truncated tetragonal rod-like morphology. All images of the sample clearly show lattice fringes of (101) plane with an interplanar distance of 3.54 Å indicating that the

TiO_2NWs have high crystallinity and single crystalline nature, which is in accordance with the XRD results. Fusing the TiO_2NWs together by calcination guarantees a good mechanical stability of the filter paper and ensures secure localization of the TiO_2NWs within the filter paper even under turbulent air flow conditions.

2. The dependency of the particle retention efficiency on thickness and porosity of the TiO_2NWs-based filter paper

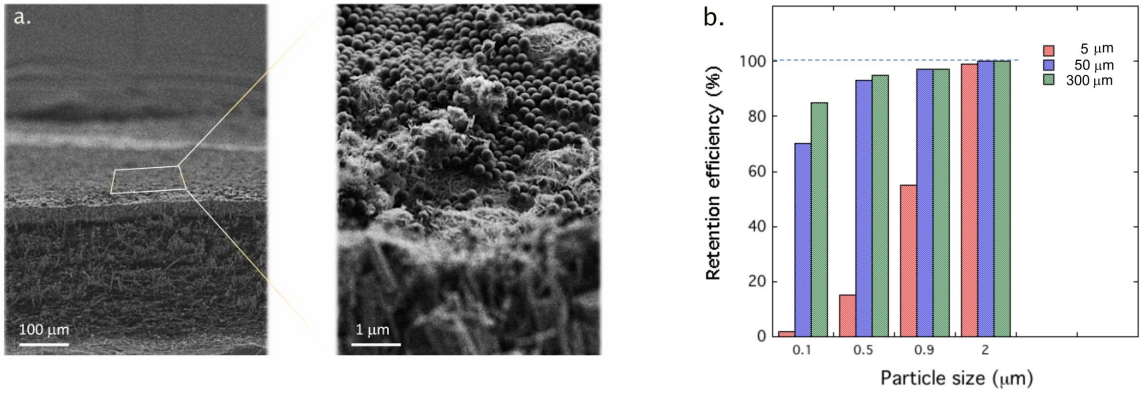

Figure S2. a) SEM image of the filter paper of 300 mm thickness with the zoomed on image showing the retained particles at its surface; b) Demonstration of the particle retention efficiency as a function of the filter paper thickness, for a suspension containing 13.7 mg/L particles of various sizes.

3. ESR characterization of ROS generation

3.1. The experimental setup for checking the propensity of the TiO_2NWs-based composite toward photo-generation of ROS in water

The propensity of the TiO_2NWs-based composite toward photo-generation of ROS was checked in the aqueous milieu using a custom-designed photo-reactor. The stable nitroxide radical, 4-Hydroxy-2,2,6,6-tetramethylpiperidine-1-oxyl (TEMPOL), was used as a target molecule for the photo-generated $OH^{\cdot}$ and $O_2^{\cdot-}$ radicals. The technique of electron spin resonance (ESR) was employed to check the photo-degradation of TEMPOL.
The schematic representation of the experimental setup is shown in Fig. S3. As indicated in the scheme, the inner wall of the tubular photo-reactor was covered with the TiO_2NWs-based composite material, which formed a photocatalytic lining. The built-in commercially-available UV lamp (Hamamatsu Photonics, operating at λ = 365 nm with power density of 16 mW/cm^2) served as a UV light source for inducing the photocatalytic processes at the surface of the TiO_2NWs-based lining.

To observe the photocatalytic formation of ROS, a volume of approximately 1 liter of 200 micromolar solution of TEMPOL in water (Milli-Q) was continuously re-circulated through the photo-reactor by the peristaltic pump. Aliquots of ~100 microliter were taken at 20-min time intervals with using the sampling valve. Subsequently, for performing the actual ESR measurements, the ~20 microliter volumes of sample aliquots were filled into 0.7 mm ID/0.87 mm OD (100 mm long) quartz capillaries (VitroCom Technical Glass, Model CV7087Q). The

ESR spectra were acquired at different time points immediately after collection of a specific sample aliquot.

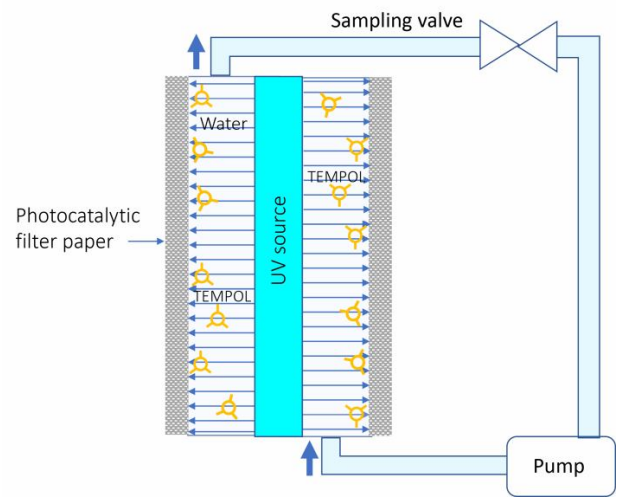

Figure S3. Schematic representation of the experimental setup used to characterize the photocatalytic properties of the TiO_2NWs-based filtering paper in the aqueous milieu. The custom-made tubular photo-reactor is equipped with a commercially-available UV light source (λ = 365 nm with power density of 16 mW/cm^2). The inner wall of the photo-reactor is covered with the composite matrix material containing the immobilized photocatalytically-active components (TiO_2NWs), which form the photocatalytic lining.

3.2. The time evolution of the ESR spectra during the photocatalytic decomposition of TEMPOL

The stable nitroxide radical, TEMPOL, was used as a target molecule for the photo-generated $OH^{\cdot}$ and $O_2^{-\cdot}$ radicals. The ESR-active TEMPOL is a water-soluble antioxidant and has been reported acting as a superoxide dismutase (SOD) mimicking agent[1]. It is generally accepted that the reactive pathways of TEMPOL with $O_2^{-\cdot}$ and $OH^{\cdot}$ radicals introduce structural changes at the 1- and 4-positions of the TEMPOL molecule, respectively[2],[3]. Acting in concert, these structural changes induce both the decay of the ESR-active TEMPOL as well as the concurrent formation of another ESR-active radical, 4-oxo-TEMPO, *i.e.* TEMPONE.

The reaction schemes of the photo-catalytic decomposition of TEMPOL and the concurrent formation of TEMPONE are shown in Fig. S4. Specifically, in Fig. S4a, the reaction scheme of the superoxide radical ($O_2^{\cdot-}$) mediated formation of the ESR-silent hydroxylamine from TEMPOL is shown. The simultaneous reaction scheme, which leads to the formation of the ESR-active TEMPONE, is depicted in Fig. S4b.

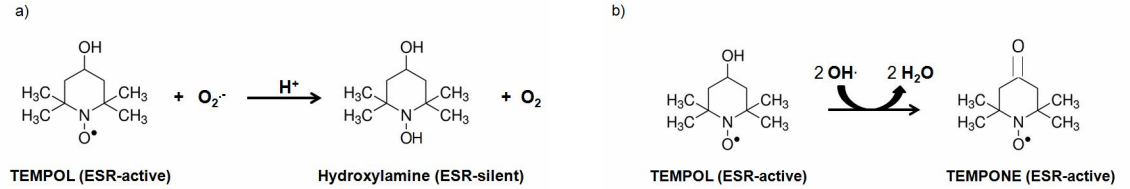

Figure S4. Mechanisms of the photo-catalytic decomposition of TEMPOL and the concurrent formation of TEMPONE. (**a**) Reaction scheme for the superoxide radical ($O_2^{\cdot-}$) mediated formation of the ESR-silent hydroxylamine from TEMPOL (adapted from W. Kudo *et al.*[4]). (**b**) Reaction scheme for the hydroxyl radical ($OH^{\cdot}$) mediated formation of the ESR-active TEMPONE (4-oxo-TEMPO) from TEMPOL (adapted from K. Saito *et al.*[5]).

In aqueous solutions, both TEMPOL and TEMPONE reveal easily detectable ESR spectra, which are characteristic for NO-centered radicals bearing one unpaired electron ($\boldsymbol{S}$=1/2). In particular, the corresponding ESR signals consist of three well resolved features resulting from the ^{14}N atom-related hyperfine splitting ($\boldsymbol{I}$=1). Due to small differences in the hyperfine splitting constants, $\boldsymbol{A}^{14}_{N}$, and spectroscopic $\boldsymbol{g}$-factor values, being of 17.1 G/$\boldsymbol{g}$=2.0057 and 16.1 G/$\boldsymbol{g}$=2.0056, for TEMPOL and TEMPONE, respectively, these two radical species can be very easily distinguished.

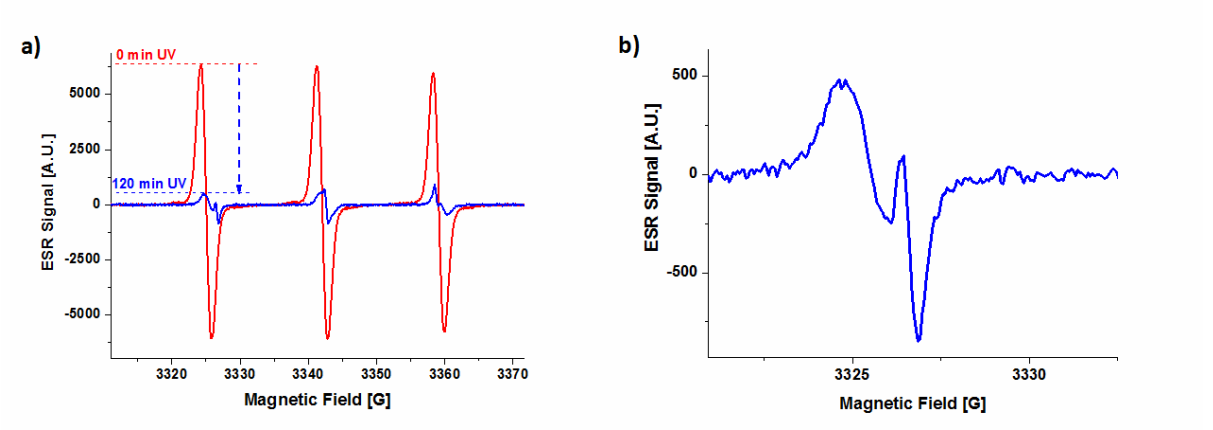

Figure S5. Photocatalytic degradation of TEMPOL in the experimental photo-reactor lined with the TiO_2NWs-based filter material. (**a**) The ESR spectrum of 200 micromolar TEMPOL before the photocatalytic cycle (**red trace**) and the complex ESR spectrum consisting of TEMPOL and TEMPONE after 120 min of UV illumination (**blue trace**). (**b**) Blowup of the low-field component of the ESR spectrum acquired after 120 min of UV illumination. The relative concentrations ratio of TEMPOL and TEMPONE is 5:1.

The example time-evolution of the ESR spectra recorded during the photocatalytic degradation of 200 micromolar TEMPOL in the experimental photo-reactor lined with the TiO_2NWs-based filter material is shown in Fig. S5. Specifically, as indicated in Fig. S5a, the characteristic ESR signal of TEMPOL (red trace) rapidly decays during the photocatalytic cycle and, after 120 min of the exposure time (blue trace), its overall ESR signal intensity decays by a factor of ~15. Moreover, as can also be seen in Fig. S5a, the resulting ESR spectrum is distorted, since it contains the admixture of the ESR signal of the photo-induced TEPMONE. This complex signal can be better seen in Fig. S5b, which presents the blowup of the low-field component of the ESR spectrum acquired after 120 min of the exposure time.

Thus, the time-evolution of the ESR spectra shown in Fig. S5 confirms that during the photo-degradation of TEMPOL, a concurrent process of formation of TEMPONE is also occurring. These both processes, *i.e.* the decay of TEMPOL and the progressive increase of TEMPONE, prove that under UV light exposure the herein synthesized TiO_2NWs–based photocatalytic material generates both $O_2^{-\cdot}$ and $OH^{\cdot}$ radicals (for reference, see the reaction schemes in Fig. S4).

3.3. Typical instrumental settings for collecting the ESR spectra

For performing ESR measurements, a cw-ESR X-band spectrometer, Bruker ELEXSYS E500 (Bruker BioSpin), equipped with a high-Q cylindrical cavity (Model ER 4122 SHQE), was used. All the ESR spectra were acquired at room temperature (293 K). The typical instrumental settings were: microwave frequency ~9.4 GHz; microwave power 0.633 mW; magnetic field sweep 120 G; magnetic field modulation frequency 100 kHz; magnetic field modulation amplitude 0.5 G; time constant 28.48 ms; spectral resolution 2048 points; conversion time 40.96 ms; resulting magnetic field sweeping time 83.89 s; two scans were accumulated per one trace.

4. Photocatalytic disintegration of DNA: AFM an electrophoresis assays - Experiment preparation

For AFM and electrophoresis assays we used a commercial DNA plasmid, pUC19. Prior to the experiments, the supercoiled pUC19 DNA plasmid was treated for a sufficient time with a nicking enzyme (Nt.BspQI) to produce the linear chains of DNA, as described in G. Witz *et al*.[6]. This procedure transformed the supercoiled (closed) strands of the pUC19 DNA plasmid into linear DNA fragments, with the lengths of 913 nm.
A 10-milliliter volume of the stock solution of TiO_2NWs in distilled water (Milli-Q ultrapure) with concentration of 0.81 mg/ml was prepared. Next, a 10-microliter volume of this stock solution of TiO_2NWs was mixed in a test tube with a 10-microliter volume of the previously prepared stock solution of the pUC19 DNA plasmid in water (with concentration of 2 ng/μl).
A control sample was prepared by 1:1 mixing the DNA stock solution with distilled water (Milli-Q ultrapure water) in another test tube. Subsequently, both test tubes were centrifuged, shaken and exposed to 365 nm UV radiation. The lamp power was set to a power density of 16 mW/cm^2 and positioned at a distance of 60 mm above the liquid surface. The radiation treatment was carried out with a following cycle: 30 sec of irradiation followed by 2 min of shaking and rotation without irradiation. This cycle avoids overheating that also can break the DNA chain.

To maintain the samples at a constant temperature and to avoid spurious decomposition of the linear fragments of DNA, the test tubes were partially immersed in a water pool, which provided a heat sink. The radiation cycles were 3, 5, 10 and 15 minutes. Prior to AFM imaging the DNA strands were separated from the TiO_2 NWs by centrifugation at 10,000 rpm

for 5 minutes. To 2 μl of the supernatant part containing the DNA (while TiO_2 NWs precipitates), 2 μl of $MgCl_2$ (10 mM) was added together with 4 μl of distilled water. The resulting suspension was deposited on a smooth mica substrate. Finally, after drying the mica substrate with nitrogen, the DNA samples were imaged by AFM and to observe the structural changes of the DNA strands upon UV exposure.
The AFM system, Model NX10 from Park Systems Corp., was employed and all measurements were performed in tapping mode using a PPP-NCSTR tip with a curvature radius < 10 nm.

The second technique used in this work for checking the variability of sizes of the DNA chain fragments was the gel electrophoresis, which, in contrast to AFM, has a more global than local character.

In this technique, the DNA fragments migrate through the agarose gel with different velocities, which depend on the applied voltage and DNA chain sizes and their characteristics, according to the following formula:
$v = E*z/f$, where v is the speed, E the electric field, z the net charge and f the frictional force. As a result of the electrophoresis process, the DNA chain fragments are separated by size and their actual locations within the gel are evidenced by means of a suitable fluorescent dye, GelRed® from Biotium.

References:

[1] H. Lu, J. Zhen, T. Wu, A. Peng, T. Ye, T. Wang, X. Yu, N. D. Vaziri, C. Mohan, X. J. Zhou, *Am. J. Physiol. Renal Physiol.* **2010**, *299*, F445.
[2] C. S. Wilcox, *Pharmacol. Ther.* **2010**, *126*, 119.
[3] D. L. Marshall, M. L. Christian, G. Gryn'ova, M. L. Coote, P. J. Barker, S. J. Blanksby, *Organic & Biomolecular Chemistry* **2011**, *9*, 4936.
[4] W. Kudo, M. Yamato, K.-I. Yamada, Y. Kinoshita, T. Shiba, T. Watanabe, H. Utsumi, *Free Radical Research* **2008**, *42*, 505.
[5] K. Saito, K. Takeshita, J.-I. Ueda, T. Ozawa, *Journal of Pharmaceutical Sciences* **2003**, *92*, 275.
[6] G. Witz, K. Rechendorff, J. Adamcik, G. Dietler, *Phys. Rev. Lett.* **2008**, *101*, 148103.